

Grain-Scale In-situ Study of Discontinuous Precipitation in Mg-Al

J. D Robson^a, A. D. Smith^b, J. Guo^a, J. M. Donoghue^a, A. E. Davis^a

^a*Henry Royce Institute for Advanced Materials, The University of Manchester, Manchester, M19 3PL, UK*

^b*TESCAN-UK, Wellbrook Court, Cambridge, CB3 0NA, UK*

Abstract

Competitive continuous and discontinuous precipitation (CP and DP) have been studied in-situ for the first time in magnesium alloys, using the Mg-Al system as an exemplar. CP forms first, and strongly affects the subsequent migration of the high angle grain boundary (reaction front, RF) behind which DP occurs. It has been demonstrated that in contrast with expectations from classical DP theory, the RF does not migrate with a steady-state velocity, but instead proceeds in a jerky stop-start fashion. Furthermore, the RF velocity is not constant but varies from grain to grain, by a factor of 4 for the conditions investigated. This growth behaviour can be explained by the interaction of the RF with CP. Whilst a mean-field model has been demonstrated to correctly predict the overall CP and DP kinetics, it is shown that the jerky motion of the RF is due to local effects. A simple model has been developed that demonstrates how the locally depleted solute field around a CP leads to arrest of a segment of the RF until sufficient diffusion occurs along it to reactivate RF motion. Zener pinning and boundary curvature also play an important, but secondary role. The results have implications for controlling DP, which is usually considered undesirable.

Keywords: Precipitation, Magnesium alloys, Discontinuous precipitation

1. Introduction

Discontinuous precipitation (DP) involves the decomposition of a supersaturated solid solution at a moving grain boundary (the reaction front), leaving in its wake a two-phase lamellar structure. It occurs in over 170 alloy systems [1] and is thus of great scientific interest. It is also practically

important, since DP usually has a deleterious effect on the mechanical, physical, and chemical properties of the alloys in which it occurs [2]. Despite its ubiquity, and intensive study (over 700 publications [1]), DP is not yet fully understood. For example, it is not currently possible to reliably predict the conditions under which DP will occur for a given alloy system, and this hampers efforts towards computational design of alloys and heat treatments.

One commercially important example of a system where DP is commonly observed is Mg-Al. This forms the basis of the industrial AZ class of alloys, the most widely used magnesium based material. Despite the ability of these alloys to form a volume fraction of precipitate phase close to 15%, the strengthening response obtained is poor; less than half that achieved in some aluminium alloys that form a much lower fraction of precipitates [3]. One reason for this is the susceptibility of Mg-Al alloys to DP. The discontinuous reaction competes with continuous precipitation (the nucleation and growth of individual particles in the grain interior). When continuous precipitation (CP) forms, it suppresses DP by reducing the supersaturation and through Zener pinning of the moving grain boundary [4–6].

Although prediction of DP is difficult, its general features are well understood. DP formation does not require a classical nucleation event [7]. It begins at a pre-existing grain boundary that undergoes migration, often with the assistance of a pre-existing grain boundary precipitate [7].

Following the initial grain boundary (reaction front, RF) motion, there is a transition period after which a steady-state is supposed to become established. Several growth models have been developed to describe steady state DP growth [7–9]. These models consider an idealized picture, where DP grows with precipitate lamellae that are equidistant, parallel to each other, and aligned normal to a planar reaction front advancing into the supersaturated matrix. This ideal picture is often far from the complex morphologies observed in practice, as recently characterized in 3-dimensions for DP in the Mg-Al system [10]. Many of the growth models do not provide a unique solution to the growth velocity for a given set of conditions (e.g. supersaturation, temperature). This is because the growth velocity is also a function of the precipitate layer spacing, which is not fixed. To find a unique solution to the velocity, an additional constraint has to be introduced. Such constraints have included the assumption that growth occurs at the fastest possible velocity [8] or optimum rate of free energy dissipation [7].

The lack of a unique solution for DP growth was solved in a model developed by King et al. [9] that predicts a single growth velocity by simultane-

ously calculating the growth of both precipitate lamellae and the interlamellar matrix assuming there are two different controlling mechanisms operating. The first is grain boundary diffusion, controlled by the lateral gradient in concentration that develops in the interlamellar matrix. The second is diffusion along the interphase boundary, controlled by gradients in curvature at the boundary interface. By assuming local thermodynamic equilibrium and diffusive flux continuity at the triple junction between phases a unique solution to the growth velocity can be found. This model has been demonstrated to give a reasonable estimate of the mean growth rate of DP regions in Mg-Al alloys [6]. These models all consider DP in isolation and do not account for the interaction between DP and CP that is common in the Mg-Al and other systems.

In addition to theoretical treatments, there have been detailed studies of DP in a range of alloy systems [1]. Some of the most revealing experiments consist of watching the development of DP in-situ in the microscope. This is typically achieved using transmission electron microscopy (TEM) combined with a heating stage [11–13]. Traditionally, TEM was necessary since other electron microscopy techniques lacked sufficient resolution to resolve the DP lamellae, which can be on the nanometer scale. These in-situ studies reveal differences in behaviour compared to the simple classical model of DP. Firstly, the RF is never flat, but always curved, so that as the DP region grows and its radius increases, the lamellae are required to branch to maintain the optimum spacing [1]. Secondly, the precipitates in the DP region are often not continuous plates, but instead have irregular or globular morphologies [1]. Finally, in some systems, growth of the RF is not smooth, but appears to proceed in a jerky stop–start fashion [13, 14].

One limitation of in-situ TEM studies is the restriction to very small volumes of material; usually only one DP region in one grain is observed in any experiment. Attempts have also been made to perform “quasi-insitu” analysis of DP growth in the scanning electron microscope (SEM) [15] in the Mg-Al system, in which the same region is tracked, but heating takes place outside the microscope. This method allows for the evolution of DP in one region to be followed, but the sampling frequency is very low. Finally, one example of an in-situ study of DP performed in the SEM with a hot stage is reported in [16] for the Al–Zn system. The focus of this study was to measure the incubation time for DP formation, and identify any potential role of grain orientation. The average growth rate was reported for all DP regions, but this was not tracked as a function of time. Additionally, at the

resolution used in the study, no CP was observed, and thus the interaction between DP and CP could not be investigated.

In the present work, in-situ heating experiments have been performed using a high resolution SEM to track the simultaneous evolution of DP and CP in the Mg-Al system. Crystallographic information has also been obtained through the use of electron back-scattered diffraction (EBSD). The growth velocities of different DP regions have been tracked over time. This provides new insights in the DP process. In particular, the interaction between DP and CP has been directly observed in-situ for the first time, and this highlights the important role that CP has in determining both the kinetics and morphology of the precipitates in the DP region, neglected in previous theories.

2. Experimental Method

The material used for this study was a commercial AZ80 alloy supplied by Luxfer MEL technologies, Manchester, UK, as a direct chill cast ingot. The nominal composition range is 7.8–9.2 Al, 0.2–0.8 Zn, 0.12–0.5 Mn, Mg (bal) wt%. A section of the alloy billet was homogenised at 400°C under an argon atmosphere using a Lenton tube furnace. This section was then rolled on a laboratory scale rolling mill from a height of 30 to 6.3 mm (total reduction of 80%) in 7 passes, using a 30 min preheat at 400°C and a 5 min reheat at 400°C between passes. Quenching in water was performed immediately after the final rolling pass. Finally, the rolled billet was solution treated at 420°C for 1 hour under an argon atmosphere and quenched once more. This produced a supersaturated solid solution microstructure so ageing could then be carried out on a test sample in-situ with an SEM heating stage.

A $2 \times 2 \times 1$ mm test sample was cut from the rolled and heat-treated billet, ground using silicon-carbide paper up to 4000 grit, polished using 3 then 1 μm diamond paste with oil-based lubricant, and finally polished using water-free 0.2 μm fumed silica. The sample was cleaned in an ultra-sonic ethanol bath between each polishing step. To produce a completely clean sample surface free of any preparation-induced deformation for SEM imaging and EBSD, a Leica EM RES102 ion beam milling system was used to remove a thin layer from the sample surface by sputtering, using two cleaning steps: 1) for 10 min at a beam angle of 12.5°, and 2) 10 min at 5°. The sample was then adhered to the SEM heating stage using Agar Scientific PELCO high-temperature carbon paste.

2.1. SEM In-Situ Heating

The experiment was conducted on a bespoke in-situ SEM testing system (Tescan and NewTec In-Situ Testing TANIST) that specialises in automated experiments with high temporal resolution. The system consisted of a TESCAN CLARA field emission gun (FEG) SEM with a Newtec FurnaSEM heating stage affixed inside that is designed so that it does not block the electron diffraction cone from the sample to an EBSD detector when the stage is tilted to 70° . Since the zinc in the AZ80 alloy sublimates at 194°C at the optimum vacuum pressure of 4×10^{-4} Pa [17], an ageing temperature of 180°C was chosen to avoid the risk of contaminating the SEM chamber and electron column. The precipitation temperature of 180°C is expected to produce a mixed microstructure of CP and DP, enabling the interaction between these modes to be studied [18].

The automated in-situ experiment was designed so that the DP and CP interactions could be studied using backscatter electron (BSE) imaging and correlated to grain boundary movement and grain misorientations using EBSD. Since EBSD scans are relatively time consuming, they were only collected before, midway, and after the heating experiment. Therefore, the precipitation evolution was studied with BSE imaging over a 20 h period at 180°C , allowed to cool to collect the midway EBSD map (after in-situ plasma cleaning of the sample), then reheated to 180°C for another $\simeq 20$ h collecting BSE images. Before the in-situ imaging experiment was started, the sample was left in the chamber to pump overnight to obtain the best vacuum possible; and imaging was started after the sample was allowed to outgas for 20 s (with the column valves closed) and a further $\simeq 1$ min was required to align the electron beam.

BSE images were collected with a four-quadrant camera at a working distance of 12 mm, using a beam accelerating voltage of 10 kV and current of 10 nA. Since the location of DP nucleation was not known a-priori in the observed microstructure, a $200 \times 200 \mu\text{m}$ area was imaged at high resolution (4096×4096 pixels) to ensure several DP nucleation events were captured and could be subsequently segmented from the dataset for more detailed study. A dwell time of $10 \mu\text{s}$ was selected to optimise both BSE signal strength and capture rate, resulting in an image collection time of $\simeq 3$ min. A bespoke MATLAB code (https://github.com/mjaykr/miscellaneous/tree/main/ACB_TIFF) was used to correct the image contrast variance across the full dataset for conversion into videos showing the areas of interest. The RF front position was tracked manually for each frame along a series of lines,

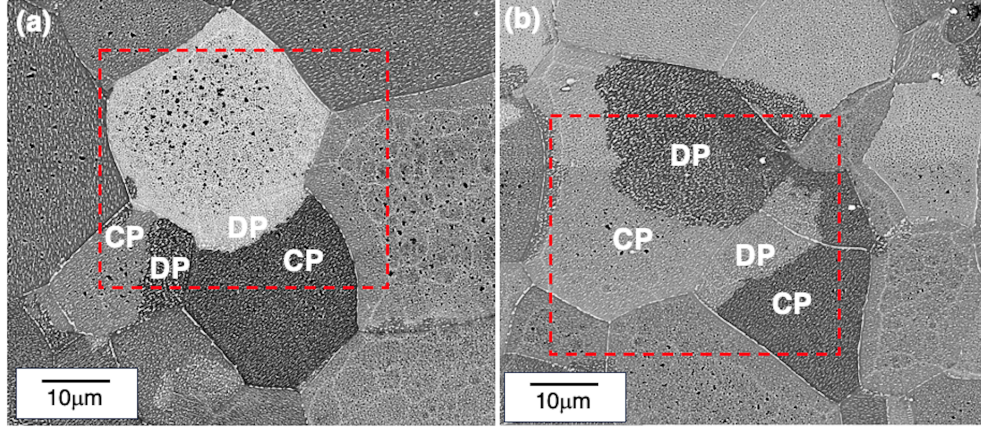


Figure 1: Overview micrographs after the in-situ experiment showing (a) area 1 and (b) area 2. Regions of discontinuous precipitation (DP) and continuous precipitation (CP) are marked. The dashed boxes indicated selected subregions for detailed analysis.

selected to be approximately normal to the final RF position. The average and maximum boundary velocities were determined from these measurements. Post-heating BSE images were also collected to study the precipitation with higher resolution using an FEI Magellan FEG-SEM with an accelerating voltage of 5 kV, a current of 0.8 nA, at a working distance of 4 mm.

EBSD scans were conducted with a beam accelerating voltage of 20 kV, a current of 20 nA, sample tilt of 70° , and a step size of $1 \mu\text{m}$, using an Oxford Instruments' Symmetry 3 EBSD detector with AZtec acquisition software. EBSD maps were processed using Oxford Instruments' AZtecCrystal software – maps are presented in inverse pole figure (IPF) colouring with respect to the rolling-normal (ND) direction.

3. Results

Two areas of the microstructure were tracked during the in-situ experiment. The final microstructures at the end of the experiment for these two regions (area 1 and area 2) are shown in Figure 1(a) and (b) respectively, recorded ex-situ by high resolution SEM. In both areas, regions of both CP and DP were observed. Sub-regions from areas 1 and 2 are shown in more detail in Figure 2. The white speckles in these images correspond to the precipitates, higher magnification images of which are presented later.

The dashed yellow lines in Figure 2 indicate the original positions of

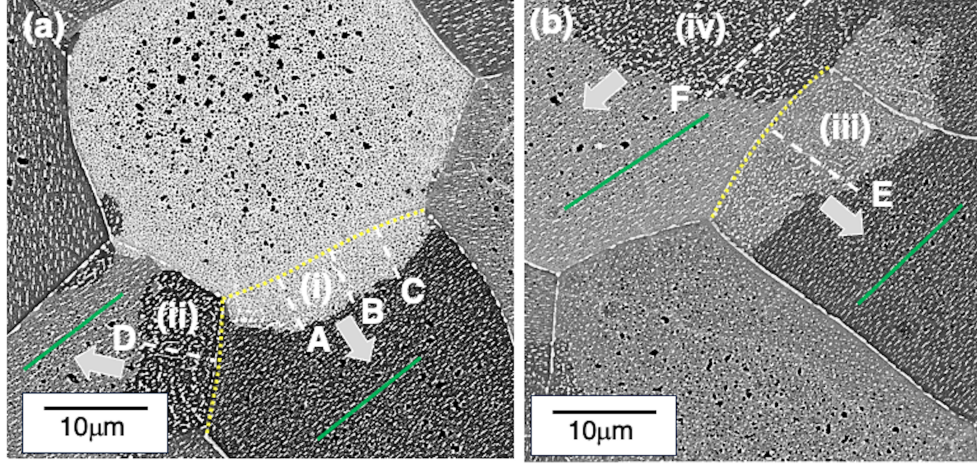


Figure 2: Subregions after the in-situ experiment within (a) area 1 and (b) area 2. The original grain boundary positions are marked as yellow dashed lines. DP regions are marked (i–iv) and paths along which the boundary velocity was measured are indicated by white dashed lines labelled A–F.

the grain boundaries for the DP regions labelled (i–iv). The arrows in this figure indicate the direction in which the boundaries (RF) moved, behind which DP formed. Paths A–F show the directions along which boundary position measurements have been made over time to track the migration of the RF during the in-situ heating experiment. The green lines are drawn approximately parallel to the 2-dimensional projection of the basal plane in each of the grains, identified by EBSD (presented later). It can be seen that there are different relationships between the direction of DP growth and the basal plane orientation of the grain being invaded. For example, DP regions (i) and (iii) grow with the RF migrating almost perpendicular to the basal plane of the grain being consumed. Region (iv) has growth by RF migration near to parallel to the basal plane of the grain being consumed. For region (ii) the RF migration direction is at an intermediate angle to the basal plane (approximately 38°).

3.1. In-situ Imaging

Snapshot images taken from the video every 50 frames are shown for the subregions of area 1 in Figure 3 and area 2 in Figure 4. The reader is also encouraged to view the full videos provided online since this reveals the boundary motion more clearly (<https://youtu.be/JAm1cLMuyTc>). Since

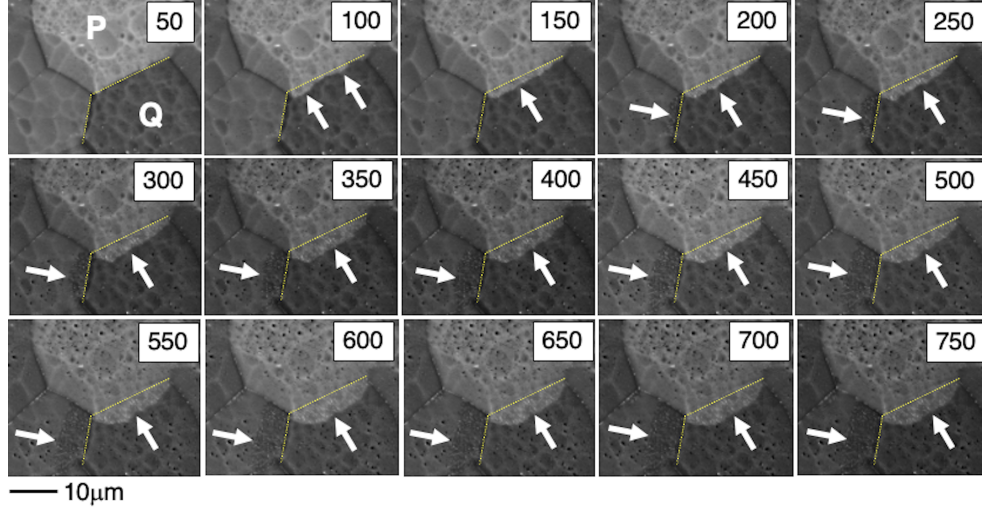


Figure 3: Snapshots from area 1 during the in-situ experiment at 50 frame increments from 50–750 frames. Dashed lines indicate the original grain boundary positions and arrows indicate the DP reaction front position.

frames were acquired every 180 s (3 minutes), by frame 50 (which corresponds to the first observation of DP) 9000 s (150 minutes) had already elapsed.

The original grain boundary positions are indicated by dashed yellow lines, and the positions of the RF are indicated by the white arrows. Area 1 provides one of the clearest examples of the progression of the RF due to the high contrast between neighbouring grains. Focussing on the region identified as (i) in Figure 2(a), it can be seen that this started from two bulges in the boundary of the lighter shaded grain (P) migrating into the darker shaded grain (Q). These bulges are visible in frame 100, and by frame 150 the boundary between bulges has also migrated, catching up with the original bulges and leading to a single RF that migrates into grain Q. This continues to evolve by further growth into grain Q until at around frame 600, the boundary stops moving, marking the maximum extent of the DP region. Similar, albeit less obvious, behaviour is observed in the snapshots of area 2.

Although difficult to see from the snapshots, it is readily apparent from the videos that the RF motion is very jerky, with long arrest times for some intervals followed by further rapid movement. In addition, not all DP regions grow at the same speed. For example, the DP region in area 2, indicated by (iv) in Figure 2(b) grew significantly faster than region (iii) in the same area. Quantitative analysis of growth rates is presented later.

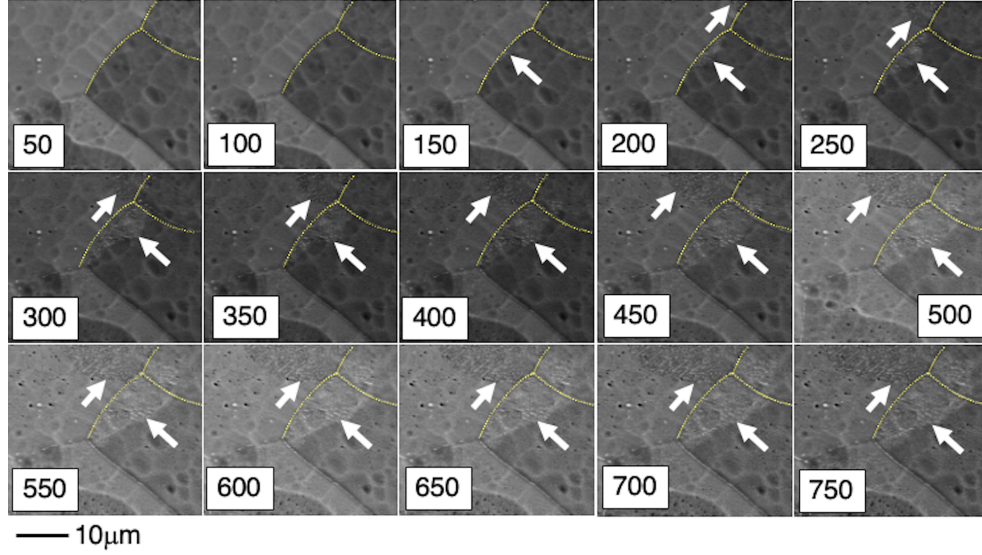


Figure 4: Snapshots from area 2 during the in-situ experiment at 50 frame increments from 50–750 frames. Dashed lines indicate the original grain boundary positions and arrows indicate the DP reaction front position.

3.2. Texture and Grain Boundary Evolution

EBSD maps of the whole specimen for the start, middle, and end states are shown in Figure 5. Unit cell hexagons are superimposed to aid interpretation of the texture. As expected, the material shows a predominantly basal texture (red), but with some grains in prismatic orientations (green), and some in intermediate orientations. The areas where DP was monitored are marked as boxes on the EBSD maps. The boundary motions associated with DP are sufficiently small that the texture is not greatly changed during the experiment, and no grain undergoes complete recrystallization. The small number of identified low-angle grain boundaries (indicated by white lines) are also unchanged during the experiment.

The map shown in Figure 6 shows the position of the grain boundaries at the start (thin lines) and end (thick lines) of the in-situ heating. Examples of boundaries that have migrated a considerable distance ($> 5 \mu\text{m}$) are highlighted with arrows. Comparing the start and end states carefully, it can be seen that some grain boundaries have moved large distances ($> 10 \mu\text{m}$) whilst others have not moved at all. There is no obvious relationship between misorientation or local texture and the boundaries that move. The

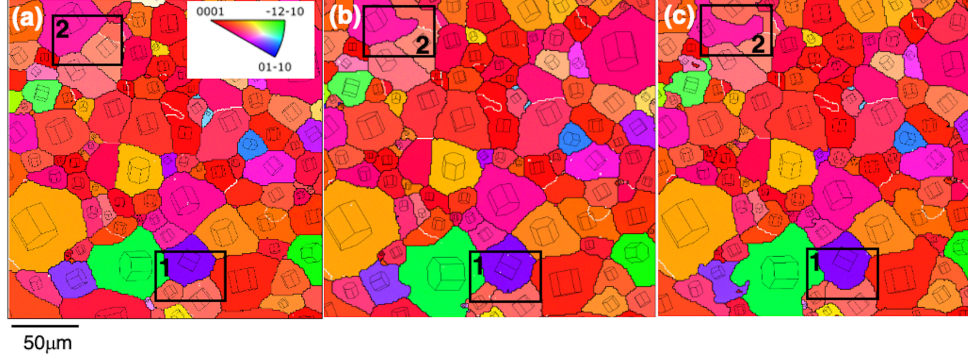


Figure 5: Overview EBSD maps (a) initial state, normal direction (ND) inverse pole figure (IPF) coloring. (b) mid-state (≈ 20 h heating) (c) final state (≈ 40 h heating). Boxes highlighting subregions in area 1 and 2 for more detailed analysis are indicated.

observations suggest that any boundary may initiate DP, except for the low angle ($< 10^\circ$) boundaries, none of which have migrated.

Figure 7 shows zoomed in EBSD maps after in-situ heating for (a) area 1 and (b) area 2. The original grain boundary positions are superimposed on these maps (yellow lines) and the regions corresponding to areas of DP are marked (i-iv) to match with Figures 3 and 4. It can be seen that DP forms behind a grain boundary that has migrated through bulging from one grain into another, so the matrix in the DP region adopts the orientation of the growing grain.

3.3. High Resolution Ex-situ Imaging

Higher magnification images showing details of the interface after the experiment (ex-situ high resolution SEM) are shown in Figure 8. Figure 8(a) shows part of the boundary for area 1, region (i). Figure 8(b) shows part of the boundary for area 2, region (iv). These regions were chosen as they demonstrate typical behaviour for two cases where the direction of movement of the RF and the basal plane of the grain being consumed are (a) near perpendicular or (b) near parallel. In both cases, the boundary can be seen to be highly tortuous, with regions where portions of the boundary appear to have become stuck and left behind. A clear example of this behaviour is seen in Figure 9, which shows a zoomed in image of the boundary for case Figure 8(a). Here, a portion of the RF has become stuck at a cluster of particles (arrowed) as the rest grows forward, leaving a “bay” that retains the orientation of the grain being consumed.

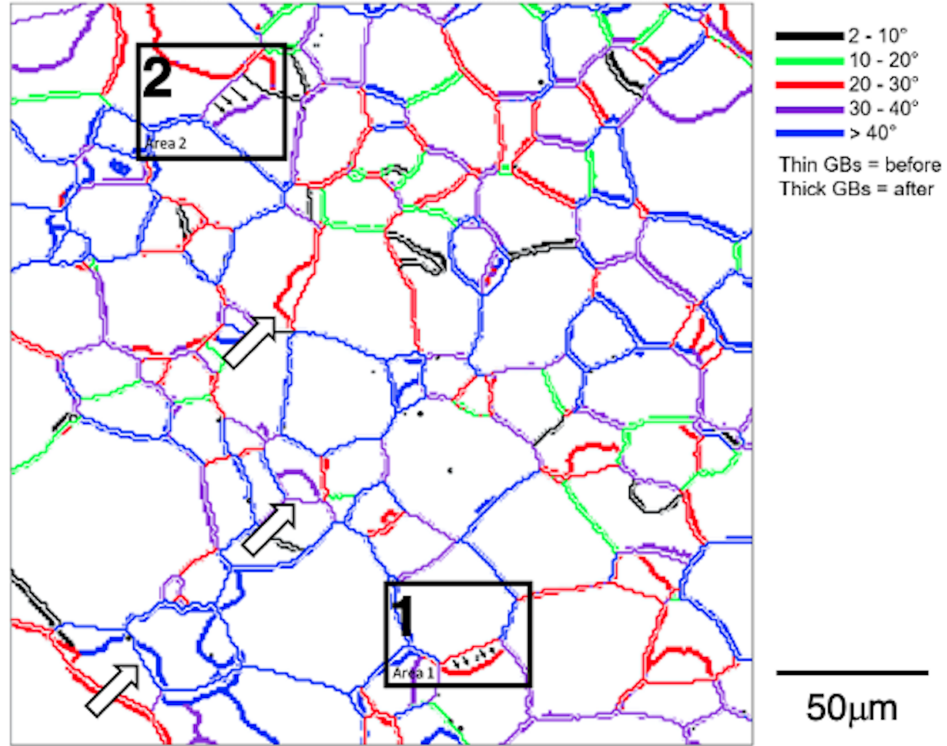


Figure 6: Boundary positions in the initial (feint) and final (bold) state. Boundaries colored according to misorientation. Boxes highlighting subregions in area 1 and 2 for more detailed analysis are indicated.

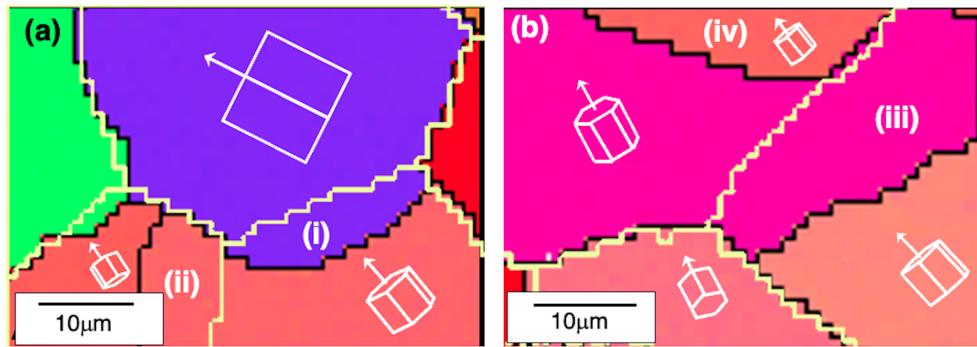


Figure 7: High magnification EBSD maps (ND-IPF coloring) showing subregions in (a) area 1 and (b) area 2. DP regions (i-iv) are highlighted. Original boundary positions are shown in yellow.

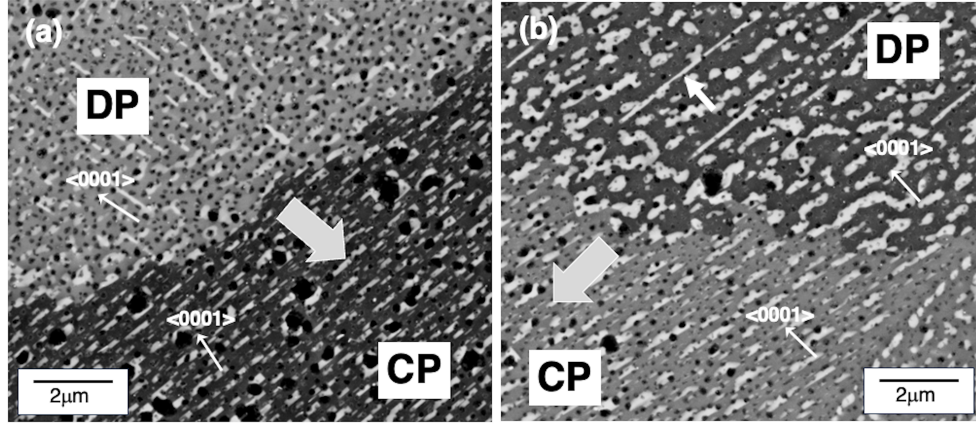


Figure 8: High magnification SEM images showing a portion of the DP reaction front after the in-situ experiment for (a) area 1, region (i). (b) Area 2, region (iv). Basal pole orientations indicated by EBSD are superimposed. The small arrow indicates a DP plate formed by elongation and merging of CPs. Large arrows indicated the RF growth direction.

Study of the videos shows how the RF interacts with the CP in the grain being consumed. A variety of complex behaviours can be observed. Evidence of these behaviours can also be seen in the post-test micrographs (Figure 8). Several key observations can be made. The first is that existing CPs are not destroyed by the passage of the RF, but instead are incorporated into the DP regions. However, they grow larger and are severely coarsened, so that the morphology can change from well defined plates to more irregular rounded shapes. Sometimes, several continuous particles will merge together as a result of this growth and coarsening process creating compound particles (as arrowed in Figure 9).

The nature of the interaction also depends strongly on the direction of the RF motion with respect to the basal plane of the grain being consumed. When the RF growth direction is near perpendicular to the basal plane of the grain being consumed (Figure 8(a)) the boundary meets the flat faces of the CPs. This can be considered an unsympathetic orientation for DP growth since the CPs will offer the maximum area for blocking movement of the RF.

The RF in Figure 8(a) is also migrating in a direction that is near perpendicular to the ideal basal habit plane for DP in the growing grain. The DP plates that form cannot maintain the preferred basal habit plane as the RF moves, but instead are aligned in a prismatic orientation. This orientation

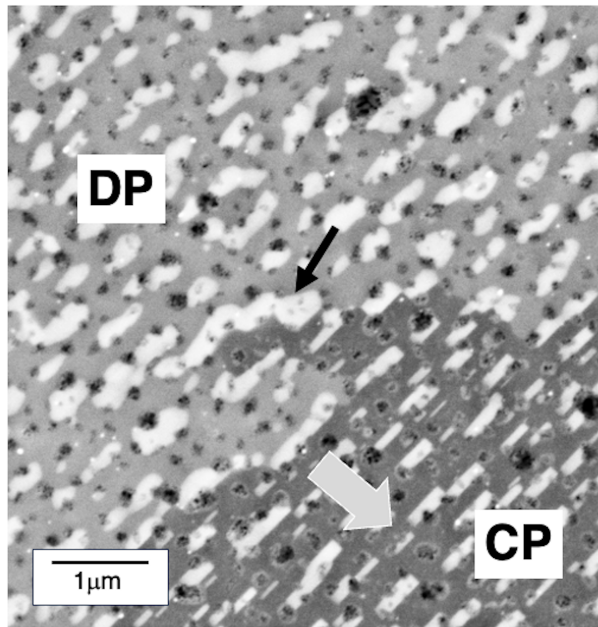


Figure 9: Detail of the DP reaction front after the in-situ experiment showing an example of boundary pinning at a cluster of CPs (small arrow). The large arrow indicates the RF growth direction.

relationship is necessary to enable the plates to grow near perpendicular to (and behind) the migrating RF.

Figure 8(b) shows a case where the RF growth direction is near parallel to the basal plane of the grain being consumed. In this case, the RF meets the tips of the CPs, minimizing their pinning effect, so this orientation is sympathetic to DP growth. The tilt between basal planes in the growing and consumed grains is small, so that the migration of the RF allows CPs to elongate along the basal plane of the growing plane behind the RF, and this can lead to merging into extended unbroken layers (see arrowed example in Figure 8(b)) that are more typical of the ideal DP structure.

3.4. Reaction Front Displacement and Velocity

The displacements of the boundary were tracked along paths A–F (Figure 2) and the resulting plots as a function of time are shown in Figure 10. Note that in all cases, there is an incubation time before boundary movement was detected, and this varied for each path. Path F corresponds to a DP region that originated outside the field of view, therefore the apparently longer incubation time in this case is an artefact because the initial growth took place out of frame. These quantitative measurements confirm the qualitative observations, including the significant difference in average boundary velocity for each path, and the jerky nature of the boundary motion. For some paths (e.g. F) boundary motion can be seen to be smoother than other paths (e.g. A, B). Paths A, B, C, and E correspond to an unsympathetic orientation between the CP and RF migration direction, as previously defined. Path F corresponds to a sympathetic orientation. Path D is an intermediate case where the RF growth direction is neither parallel nor perpendicular to the CP habit plane in the consumed grain.

It can be seen that for all paths the boundary positions had reached a long period without further movement at the end of the experiment,. The measured maximum and mean boundary velocity for each of the paths A–F (defined ignoring the incubation time and the final static period) are shown in Table 1. The maximum arrest time was recorded for path B, where the boundary stopped moving for 74 frames, $t = 13320 \pm 180$ s (3.7 hours), before re-starting.

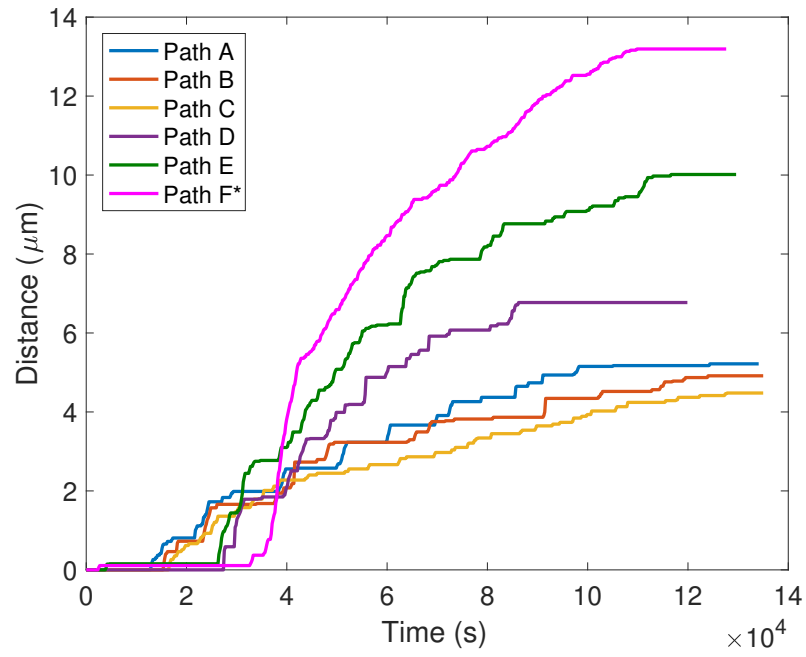


Figure 10: Measured position of the DP reaction front as a function of time along paths A–F. Path F corresponds to a DP region that initiated outside the field of view.

Path	Orientation	Max. velocity (nm s^{-1})	Mean velocity (nm s^{-1})
A	U	1.4	0.059
B	U	3.0	0.037
C	U	0.6	0.039
D	I	2.8	0.114
E	U	1.6	0.109
F	S	2.5	0.168

Table 1: Measured maximum and average boundary velocities for paths A–F (Figure 2), identifying whether the path corresponds to a sympathetic (S), intermediate (I), or unsympathetic (U) orientation (see text for details).

4. Discussion

This is, to our knowledge, the first in-situ study of discontinuous precipitation in a magnesium alloy also containing CP. Time-resolved in-situ observation offers insights into the growth process that are not available by ex-situ study of the final microstructure. This includes revealing the jerky stop-start motion of the RF not expected from classical DP theory.

Another key observation is that CPs are not dissolved at the RF, but instead become incorporated in the DP regions, coarsening rapidly as part of this process. The resulting precipitate morphologies in the DP region depend on the orientation relationship between the RF migration direction and the basal plane orientation of the grain being consumed by DP. As already discussed, two extreme behaviours can be identified, where other cases are intermediate between these extremes. The sympathetic case occurs when the RF meets the lath shaped CPs at their tips. In this orientation, the Zener pinning effect of the precipitates is minimised.. The unsympathetic case occurs when the RF meets the CPs at their flat faces, in this orientation, the Zener pinning effect is maximized. The aspect ratio of the CPs (length/thickness) measured in the present study was approximately 10, which is consistent with previous work [19]. For this aspect ratio, the Zener pinning effect of precipitates in the unsympathetic orientation is approximately 25 times greater than that in the sympathetic orientation, as calculated using the equations provided by Nes et al. [20].

When the RF encounters CP in an unsympathetic orientation (Figure 8(a)), it can grow along its long axis by fast diffusion down the RF, but only whilst the boundary is in contact with the precipitate. The precipitates will then

continue to coarsen in the through thickness direction as the RF moves away, and this leads to a complex morphology that combines both the original elongation of the CP and the new perpendicular growth. In addition, new DP also forms that is aligned antiparallel to the RF migration direction. In all cases, these new precipitates are in contact with one or more of the original CPs, suggesting they do not nucleate from the matrix but instead grow from a pre-existing particle. This is consistent with the understanding that the barrier for precipitate nucleation is large in this system [3]. In the example shown in Figure 8(a), the DP plates formed in this way have a prismatic rather than basal habit plane. This is necessary to allow the DP plates to grow behind and approximately perpendicular to the migrating RF boundary, as expected from classical theory. A prismatic habit for $\text{Mg}_{17}\text{Al}_{12}$ in Mg–Al alloys has been previously reported [19] and a small fraction of CP naturally forms this way, suggesting the energy penalty for this orientation over the basal habit is not high [19].

When the RF encounters CPs in the sympathetic orientation (Figure 8(b)) they can grow by lengthening further behind the migrating RF and merging into plates. Solute is most easily precipitated by attaching to and extending the existing CPs rather than nucleating new DP. Solute will diffuse rapidly down the the RF by grain boundary diffusion, and will attach to the CP causing it to extend in a direction antiparallel to the RF migration direction. In the case shown in Figure 8(b), the orientation of the growing grain is such that the basal habit plane can be maintained in the DP region.

In both the sympathetic and unsympathetic case, the preferred growth direction of the plates in the DP region is determined by, and is antiparallel to, the RF migration direction. By growing antiparallel to the RF migration direction, the precipitate can continue to be fed solute by grain boundary diffusion as it moves, as in classical DP growth theory [7]. The habit plane the DP adopts appears to be chosen to most closely meet this requirement. A basal habit plane for the DP will arise when the basal plane of the growing grain is near parallel to the RF migration direction. A prismatic DP habit plane occurs when the basal plane of the growing grain is near perpendicular to the RF migration direction. Based on previous observations [19], it is suggested that both the basal and prismatic habits are strongly energetically favourable, with only a small difference between them. Therefore, the plates will adopt one of these habits, even when this results in an alignment that is not perfectly perpendicular to the RF (as assumed in classical DP theory). Since the plates in the DP regions are formed from the pre-existing

CP, their spacing depends on the original CP spacing, rather than being determined solely by a balance of processes at the RF, as assumed in classical DP theory [7, 9].

4.1. Classical Global Kinetic Model

Although it is clear from the observations that the formation of DP with pre-existing CPs is more complex than the ideal assumed in DP growth theory, it is still useful to compare the present results with predictions based on classical modelling. For this, code previously developed to model competitive DP and CP in the Al-Mg system was used [6], with full details given elsewhere [6]. In brief, the model considers competitive DP and CP by combining a classical nucleation, growth, and coarsening model for CP based on the Kampmann and Wagner numerical (KWN) framework [21] and a DP model based on the Tu and Turnbull [22] nucleation mechanism and the growth theory of Klinger et al. [9]. The models are coupled to capture the interactions between CP and DP. CP can slow or stop the growth of DP by removing supersaturated solute from the matrix and by Zener pinning. DP suppresses CP by reducing the availability of untransformed volume. The model is mean-field in nature; the solute is assumed to be uniformly depleted in the untransformed matrix at all times. The model also does not capture the jerky motion of the boundary. Nevertheless, it can provide useful insights into the competition between CP and DP, and give a theoretical prediction of the DP boundary migration velocity to be compared with experiment.

The model predictions for the alloy composition and ageing temperature used in this study are shown in Figure 11. Figure 11(a) shows the calculated evolution of CP and DP, correctly predicting that a mixture of CP and DP should develop for these conditions. Consistent with the observations, the CP forms first and reaches a maximum volume fraction after 38450 s (10.7 h). DP also forms rapidly, evolving in competition with CP. The initial DP growth velocity was predicted to be 9.1 nm s^{-1} . As the CP evolves, it removes solute from the matrix, which is predicted to decrease the growth velocity of the DP as shown in Figure 11(b). However, the residual solute in the matrix is predicted to be sufficient to continue to drive DP growth, albeit at a much reduced velocity (0.19 nm s^{-1}). The DP is predicted to consume some of the CP, which explains why the predicted volume fraction of CP decreases after reaching a maximum. DP is then predicted to continue growing reaching a predicted volume fraction at the end of the experiment of 11%. The model was run with and without the Zener pinning effect of CP on

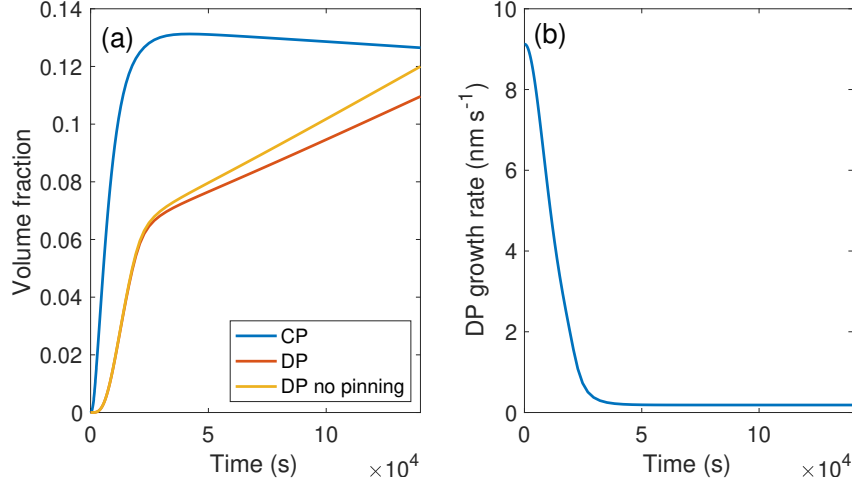


Figure 11: Predictions of a classical kinetic model for competitive DP/CP formation for the experimental conditions in the present study [6] (a) volume fraction evolution (b) DP growth velocity.

DP (ignoring the effect of CP precipitate shape and treating the precipitates as equivalent spheres [6]) demonstrating the average Zener pinning effect is quite small [6]. In summary, the mean field model correctly predicts there will be a mix of CP and DP for the composition and temperature used in this study, and predicts that the DP will grow to consume some of the CP as observed. It predicts a DP growth velocity that is on the same order as that measured experimentally (comparing the steady state model predicted velocity at long times with the mean velocity measurements). However, it is not able to capture more complex effects. In particular, the model does not predict the jerky motion of the RF and it does not account for the anisotropy of DP growth depending on the relationship between the RF migration direction and CP orientation. This suggests that these phenomena can only be explained by a full consideration of local and not just mean-field effects.

4.2. Local Solute Distribution Effect

To consider in more detail the local interactions that occur when the RF interacts with CP, it is useful to simplify to the case of a single precipitate interacting with the boundary. This situation is shown schematically in Figure 12 where the pressures and fluxes controlling the DP reaction front interacting with a continuous precipitate are indicated. The forward movement

of the boundary is driven by the pressure due to the solute supersaturation in the matrix (P_{ss}). This pressure depends on the local solute environment around the RF. In the vicinity of the continuous precipitate, the solute is depleted and P_{ss} is reduced, as indicated schematically by the length of the vectors marked in Figure 12. As the RF approaches the particle, it will interact with the locally depleted solute field, leading to a difference in growth velocity along its length. This will cause the RF to become curved, which will be resisted by a curvature induced pressure due to the grain boundary energy γ_{gb} . At the same time, grain boundary solute diffusion will occur, driven by the concentration difference between the enriched regions remote from the continuous precipitate and the depleted region in its vicinity (J_{Al}). This will lead to a time-dependent increase in P_{ss} along the solute depleted RF as the local supersaturation increases.

As the RF moves, it will eventually intersect the continuous precipitate, at which point Zener pinning will add a retarding pressure to its motion (P_z). In regions where the retarding pressures on the boundary exceed the driving pressure, the boundary will arrest. However, as P_{ss} increases due to solute enrichment of the RF, the forward driving pressure on arrested segments of the boundary will increase. Combined with the curvature pressure pulling the lagging portion of the boundary forward, this will eventually exceed the retarding pressures, unpinning the RF.

This proposed mechanism can explain the observed jerky RF migration behaviour. However, to demonstrate this mechanism in operation, a simple model was developed. The model considers the DP reaction front interacting with a single continuous, as in Figure 12. The continuous precipitate was taken as $1\mu\text{m}$ in length with a 10:1 length to thickness aspect ratio. The solute field around this precipitate was calculated using a method presented by Mou and Howe [23] for an ellipsoid precipitate, with the composition of the precipitate taken as stoichiometric $\text{Mg}_{17}\text{Al}_{12}$ and local equilibrium assumed at the interface [6].

The calculated solute field, plotted as normalized supersaturation ($= 1$ when all of the Al is in solution and 0 for the equilibrium aluminium concentration in solution) is shown in Figure 13(a). The precipitate centre is at $(0, 0)$ and due to symmetry only one quadrant of the solute field is shown. It can be seen that even though the particle is anisotropic, the solute depletion field becomes close to isotropic as the distance from the particle increases. The region of reduced supersaturation extends far from the precipitate and within $1\mu\text{m}$ in all directions is less than half of the far-field value.

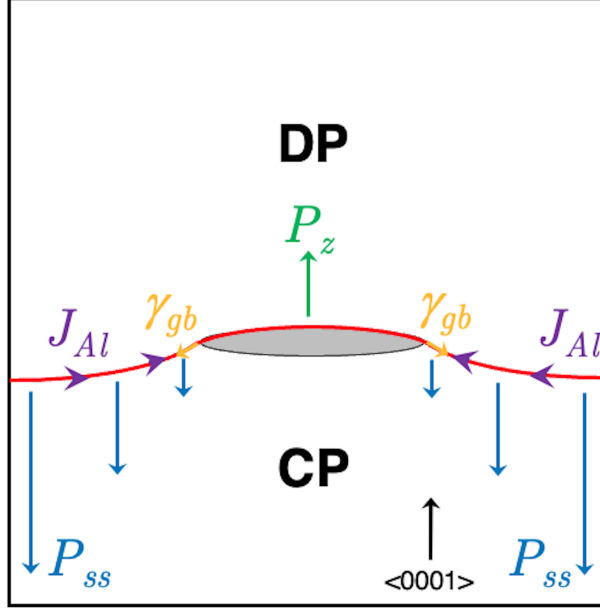


Figure 12: A sketch showing the pressures and fluxes acting on the DP reaction front as it encounters a continuous precipitate.

The solute field can be directly used to calculate the effect on the local RF velocity using the growth model of Klinger et al. [6, 9]. The resulting growth velocity contours (in nm s^{-1}) are shown in Figure 13(b). Close to the particle, where the solute is depleted, the predicted DP growth velocity is greatly reduced. The zero velocity contour (no RF migration without enrichment) extends a significant distance away from the particle (600 nm in the x -direction and 400 nm in the y -direction). This implies that in the absence of any solute diffusion, the RF would arrest ahead of the precipitate, even before Zener pinning becomes operative.

Diffusion through the lattice is very slow, at the temperature used in the experiment (180°C), a simple \sqrt{Dt} estimate gives a total lattice diffusion distance for Al of 470 nm for the entire experiment (see [6] for parameters). For the maximum arrest time observed in the experiment, the lattice diffusion distance is less than 150 nm. Therefore, rapid diffusion along the RF is necessary to redistribute solute and restart growth. According to this mechanism, It is the time dependency of the necessary solute redistribution that controls the arrest time of the RF and leads to the observed jerky motion.

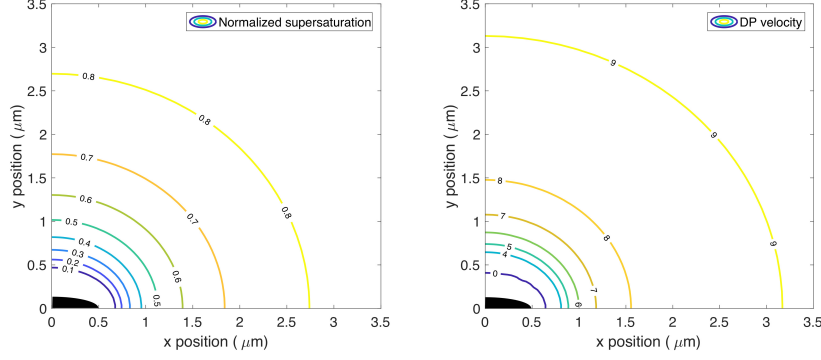


Figure 13: (a) The calculated normalized supersaturation of Al around a plate shaped precipitate of total length $1\text{ }\mu\text{m}$ and aspect ratio 10 centred at (0,0) and elongated along the x -axis. (b) The calculated DP growth velocity associated with the solute field shown in (a).

4.3. Boundary Tracking Model

These ideas were integrated into a simple boundary tracking model. The purpose of this model is to determine the consequences of the physical mechanisms described on the RF motion. It is not expected to be quantitatively accurate because several of the required input parameters (such as the grain boundary diffusivity of Al in Mg) are not well known. The model considers an initially flat RF at a distance far from a continuous precipitate, where the effect of solute depletion is not felt. The boundary is then allowed to grow towards the continuous precipitate and into the solute depleted region surrounding it. The boundary is modelled as a series of 100 nodes, tracked numerically with a small timestep ($\Delta t = 16\text{ s}$). The net pressure at each node is calculated from each contributions identified in Figure 12. The forward pressure P_{ss} is determined from the thermodynamic driving due to the local supersaturation [6]. When the boundary nodes lie at positions occupied by the continuous precipitate, a backward Zener pinning pressure is applied, P_z , otherwise $P_z = 0$. Finally, when the boundary becomes curved, a curvature pressure (P_c) will act. This will be in the forward direction on lagging boundary segments and backward direction on advancing segments. Local curvature between nodes was estimated using a MATLAB script due to Moreno [24]. Solute diffusion between nodes along the RF from high to low concentration regions is determined by numerical solution of Fick's second law of diffusion in 1-dimension using the MATLAB pdepe function.

The grain boundary diffusion coefficient of Al in Mg, which is required to solve this problem, was estimated as approximately 3 orders of magnitude greater than the lattice diffusion coefficient based on extrapolation of the experimental data due to Das et al. [25].

The boundary velocity at each node is then the sum of the various pressures acting at each node multiplied by the grain boundary mobility:

$$v = M_{gb} (P_{ss} + P_c - P_z) \quad (1)$$

Where M_{gb} is the grain boundary mobility, given by the usual Arrhenius expression as a function of temperature, the parameters for which are given in [6].

The pressure driving boundary growth (P_{ss}) is equivalent to the free energy change per unit volume due to removing supersaturated solute into DP. This was calculated using Calphad methods (JMatPro with the MGDATA database) . Experimentally, it has been shown that DP does not completely deplete the supersaturated solute (i.e. it does not leave the matrix at a uniform mean solute level) [26]. Therefore, the total free energy change was scaled by 0.5 to account for this effect. This scaling is estimated from the experimental supersaturation measurements of [26], its precise value does not affect the results. The Zener pinning pressure (P_z) was calculated as shown in [20], with the required grain boundary energy for this (and calculation of P_c) given in [6].

Figure 14(a) shows the predicted position of the RF as it moves through the non-uniform solute field surrounding a continuous precipitate. Each line corresponds to the RF position after the indicated growth time. Consistent with expectations, the initially planar boundary will become curved as the boundary segments in regions of high supersaturation grow ahead of those in regions of low supersaturation.

As the continuous precipitate is approached, the RF migration rate for nodes near the precipitate drops. Consistent with previous calculations [6], solute depletion is more significant in producing RF retardation than the direct Zener pinning effect. This can be further understood by comparing the pressures arising from the solute supersaturation and Zener pinning, as shown in Figure 14(b). In regions of the matrix where Al is fully supersaturated ($c_{Al} = 0.08$ at%), the driving pressure due to supersaturation is over 10 times greater than the Zener pinning pressure. It requires a drop in the local Al concentration to less than $c_{Al} = 0.023$ at% before the Zener pinning pressure

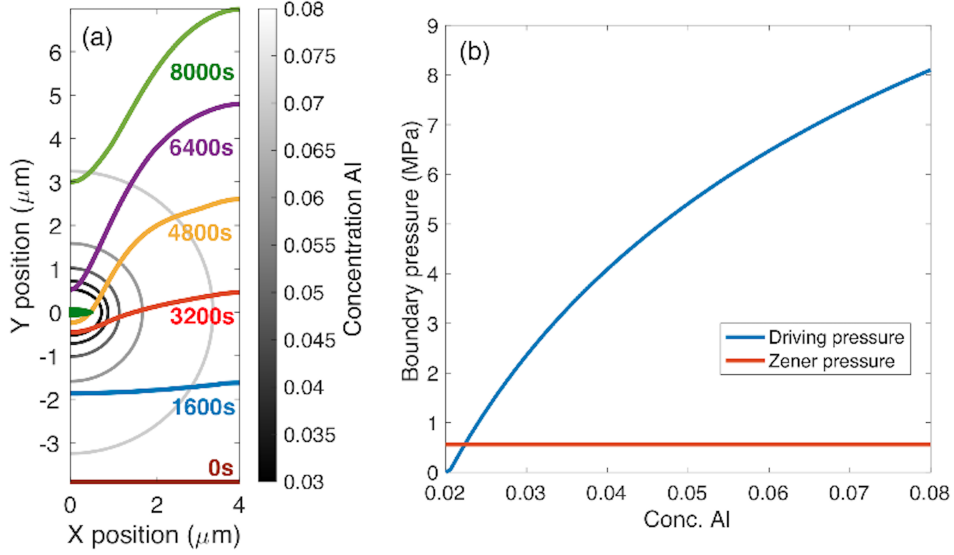


Figure 14: (a) Predicted positions of the DP reaction front evolving over time migrating through the non-uniform solute field and past a continuous precipitate centred at (0,0). (b) The pressure driving boundary migration due to solute supersaturation as a function of matrix aluminium concentration (P_{ss}) and the retarding pressure due to the Zener particle pinning effect.

exceeds the RF driving pressure. Therefore, only a small enrichment of solute is needed before the Zener pinning pressure can be overcome.

As the RF distant from the continuous precipitate advances, the curvature effect will contribute to dragging the lagging segments forward. The growth of this lagging portion accelerates as it moves into regions of greater supersaturation. This will be observed as jerky RF migration behaviour, as seen in the experiment. Although the model is not quantitatively accurate, the predicted arrest time of the boundary in the vicinity of the continuous precipitate (defined as the time over which the boundary moves less than a detection limit of $0.1 \mu\text{m}$) is 1200 s, on the same order as the shorter arrest times observed in the experiment. The mechanism captured by the model is thus a plausible explanation of the observed stop-start behaviour. It confirms that the hypothesis suggesting solute diffusion down the RF to restart its motion controls the kinetics of the arrest periods is consistent with the experimental observations.

In the experiment, the boundary is moving through a field of particles

rather than past an individual precipitate. The interaction of a grain boundary with a distribution of precipitates is a complex problem [20], but more sophisticated computer simulations have verified that the basic ideas of classical Zener theory are valid [27]. There will be local regions where the particles are closer together and the retarding effect is greatest, causing the boundary to arrest. In other regions, where the particles are further apart and the solute supersaturation is greater, the boundary will continue to move. The parts of the boundary that grow ahead will help to pull the lagging parts forward due to the curvature pressure. The basic ideas from the single precipitate case are therefore expected to apply to the real case of a distribution of particles, but with the additional complexity that any non-uniform distribution of CP will also be important.

5. Conclusions

The growth of discontinuous precipitation (DP) in competition with continuous precipitation (CP) has been studied in-situ for the first time in magnesium alloys. The alloy system used, Mg–Al, exhibits both CP and DP modes. Their interaction is critical in determining the microstructure formed after processing and heat treatment of commercial AZ magnesium alloys. The observations from the in-situ observations have been compared with predictions of a classical model for DP and CP growth, and with a new model that considers the local interactions between a migrating DP reaction front (RF) and a single continuous precipitate. The following conclusions may be drawn from this work:

1. DP is initiated when one grain bulges into its neighbour, so that the orientation of the matrix in the DP region adopts that of the growing grain.
2. All high grain angle boundaries ($> 10^\circ$ misorientation) appear susceptible to initiating DP. No DP forms at low angle grain boundaries.
3. The RF behind which DP forms does not grow with a constant velocity, but instead migrates with a jerky stop-start motion. The arrest times can be long, on the order of several hours.
4. The mean growth velocity of the DP regions can vary significantly (by a factor of 4) between grains.
5. CPs are not dissolved at the RF, but become incorporated into the DP region, coarsening and changing shape during this process.

6. Fastest mean growth velocities are measured for a sympathetic growth orientation. This corresponds to a case where the RF meets the CPs at their tips, resulting in the minimum pinning effect and enabling the CPs to grow behind the RF by solute addition to the tips.
7. Slowest mean growth velocities are measured for an unsympathetic growth orientation. This corresponds to a case where the RF meets the CPs at their flat faces, resulting in a maximum pinning effect and requiring new DP plates to form perpendicular to the flat faces of the CP.
8. The DP plates will adopt either a prismatic or basal habit plane, depending on which is best aligned to allow their growth to be sustained by RF migration.
9. Since the layers observed in the DP structure form from CPs, their spacing depends on the CP distribution before interaction with the RF.
10. A simple classical mean-field solute model can correctly predict the mixed CP and DP precipitation seen in the present study and also the consumption of some of the CP by DP. It cannot capture the jerky growth behaviour or the orientation effect on DP growth. These require consideration of local interaction effects.
11. A qualitative model has been developed to predict the interaction of the RF with a single CP. The model demonstrates that the RF stops migrating in the vicinity of the CP due to local solute depletion. The RF will only move again once sufficient solute has diffused down it to provide the necessary supersaturation to drive it forward. This is assisted by the curvature pressure, but retarded by the Zener pinning pressure at the CP.
12. The model provides a physical explanation of the jerky stop-start motion of the RF. It demonstrates that solute supersaturation and solute redistribution by grain boundary diffusion are the key mechanisms that control the DP growth velocity when in competition with CP.

6. Data statement

The in-situ movies, code, and data presented here are available from LightFORM repository (<https://zenodo.org/communities/lightform/>). The in-situ movies can also be viewed at <https://youtu.be/JAmlcLMuyTc>.

7. Acknowledgement

The authors are grateful to the EPSRC for financial support through the associated programme grant LightFORM (EP/R001715/1). J. D. Robson is grateful to DSTL and the Royal Academy of Engineering for funding through the DSTL/RAEng Chair in Alloys for Extreme Environments RC-SRF2021124. Luxfer MEL technologies are thanked for the provision of the alloy used in this study, D. Strong is thanked for conducting the rolling, and M. Kumar for the contrast correction code.

References

- [1] I. Manna, S. Pabi, W. Gust, Discontinuous reactions in solids, *International Materials Reviews* 46 (2) (2001) 53–91.
- [2] D. B. Williams, E. P. Butler, Grain boundary discontinuous precipitation reactions, *International Metals Reviews* 26 (1) (1981) 153–183.
- [3] C. R. Hutchinson, J.-F. Nie, S. Gorsse, Modeling the precipitation processes and strengthening mechanisms in a Mg-Al-(Zn) AZ91 alloy, *Metallurgical and Materials Transactions A* 36 (8) (2005) 2093–2105.
- [4] H. Aaronson, J. Clark, Influence of continuous precipitation upon the growth kinetics of the cellular reaction in an al-ag alloy, *Acta Metallurgica* 16 (1968) 845–855.
- [5] E. Hornbogen, Systematics of the cellular precipitation reactions, *Metallurgical and Materials Transactions B* 3 (1972) 2717–2727.
- [6] J.D. Robson, Modeling competitive continuous and discontinuous precipitation, *Acta Materialia* 61 (2013) 7781–7790.
- [7] R. W. Cahn, P. Haasen, E. J. Kramer, *Materials Science and Technology: A Comprehensive Treatment Phase Transformations in Materials*, Vol. 5, VCH, 1990.
- [8] H. M., On theories of growth during discontinuous precipitation, *Metall. Trans. A* 3 (1972) 2729–2741.
- [9] L. M. Klinger, Y. J. M. Brechet, G. R. Purdy, On velocity and spacing selection in discontinuous precipitation—i. simplified analytical approach, *Acta Materialia* 45 (1997) 5005 – 5013.

- [10] J. Robson, M. Lawson, J. Donoghue, J. Guo, A. Davis, Discontinuous precipitation in Mg-Al alloy studied in 3-dimensions, *Scripta Materialia* 227 (2023) 115265.
- [11] V. Ramaswamy, E. P. Butler, P. R. Swann, Direct observation of discontinuous precipitation in Al-28at%Zn, *Journal of Microscopy* 97 (1973) 259–268.
- [12] K. Tashiro, G. R. Purdy, In situ observations of chemically induced grain-boundary migration and discontinuous precipitation in the aluminum-zinc system, *Metallurgical Transactions A* 20 (1989) 1593–1600.
- [13] S. Abdou, M. El-Boragy, G. Solorzano, W. Gust, B. Predel, In-situ study of discontinuous precipitation in Al-15 at.% Zn, *Scripta materialia* 34 (1996) 1431–1436.
- [14] M. Chronowski, P. Zięba, On the go-and-stop motion of the discontinuous precipitation front, *Archives of Civil and Mechanical Engineering* 20 (2020) 20–35.
- [15] K. L. Zhang, H. Z. Li, X. P. Liang, Z. Chen, Z. X. Zhao, H. Tao, X. W. Zhou, Effect of aging time on discontinuous precipitates, continuous precipitates and mechanical properties of AZ80a magnesium alloy, *Transactions of Nonferrous Metals Society of China* 32 (2022) 2838–2851.
- [16] P. Zięba, M. Faryna, M. Chronowski, Combined in situ and EBSD studies of discontinuous precipitation in Al-22 at.%Zn alloy, *Materials Characterization* 157 (2019) 109889.
- [17] M.Schmid, Vapor pressure calculator, https://www.iap.tuwien.ac.at/www/surface/vapor_pressure, retrieved 7/2023 (2023).
- [18] D. Duly, J. P. Simon, Y. Brechet, On the competition between continuous and discontinuous precipitations in binary Mg-Al alloys, *Acta Metallurgica et Materialia* 43 (1995) 101 – 106.
- [19] S. Celotto, TEM study of continuous precipitation in Mg-9 wt% Al-1 wt% Zn alloy, *Acta materialia* 48 (2000) 1775–1787.

- [20] E. Nes, N. Ryum, O. Hunderi, On the Zener drag, *Acta Metallurgica* 33 (1985) 11–22.
- [21] R. Wagner, R. Kampmann, Homogeneous second phase precipitation, *Phase Transformations in Materials* 5 (1991) 213–303.
- [22] K. N. Tu, D. Turbull, Morphology of cellular precipitation of tin from lead-tin bicrystals, *Acta Metallurgica* 15 (1967) 369–376.
- [23] Y. Mou, J. Howe, Diffusion fields associated with size and shape coarsening of oblate spheroids, *Metallurgical and Materials Transactions A* 28 (1997) 39–50.
- [24] M. Moreno, Discrete Curvature, Normals and Evolute (<https://www.mathworks.com/matlabcentral/fileexchange/107929-discrete-curvature-normals-and-evolute>), MATLAB central file exchange. retrieved July 14, 2023.
- [25] S. K. Das, N. Brodusch, R. Gauvin, I.-H. Jung, Grain boundary diffusion of al in mg, *Scripta Materialia* 80 (2014) 41–44.
- [26] D. A. Porter, J. W. Edington, Microanalysis and cell boundary velocity measurements for the cellular reaction in a Mg-9% Al alloy, *Proceedings of the Royal Society A: Mathematical, Physical and Engineering Sciences* 358 (1978) 335–350.
- [27] M. Miodownik, E. A. Holm, G. N. Hassold, Highly parallel computer simulations of particle pinning: Zener vindicated, *Scripta Materialia* 42 (2000) 1173–1177.